ESD-TR-87-082

Technical Report
777

Cramér-Rao Bounds on the Accuracy of Location and Velocity Estimations Using CCD Optical Sensors

Y. Chen

2 November 1987

Lincoln Laboratory
MASSACHUSETTS INSTITUTE OF TECHNOLOGY
LEXINGTON, MASSACHUSETTS

Prepared for the Department of the Air Force
under Electronic Systems Division Contract F19628-85-C-0002.

The work reported in this document was performed at Lincoln Laboratory, a center for research operated by Massachusetts Institute of Technology, with the support of the Department of the Air Force under Air Force Contract F19628-85-C-0002.

The views and conclusions contained in this document are those of the contractor and should not be interpreted as necessarily representing the official policies, either expressed or implied, of the United States Government.

The ESD Public Affairs Office has reviewed this report, and it is releasable to the National Technical Information Service, where it will be available to the general public, including foreign nationals.

This technical report has been reviewed and is approved for publication.

FOR THE COMMANDER

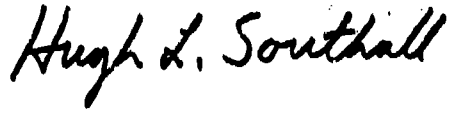

Hugh L. Southall, Lt. Col., USAF
Chief, ESD Lincoln Laboratory Project Office

MASSACHUSETTS INSTITUTE OF TECHNOLOGY
LINCOLN LABORATORY

CRAMÉR-RAO BOUNDS ON THE ACCURACY OF LOCATION AND VELOCITY ESTIMATIONS USING CCD OPTICAL SENSORS

Y. CHEN
Group 27

TECHNICAL REPORT 777

2 NOVEMBER 1987

LEXINGTON MASSACHUSETTS

ABSTRACT

A moving point-target generates a non-circular image on a CCD photo-detector focal plane. Using a two-dimensional Gaussian signal model, we have derived the Cramér-Rao lower bounds for target location and velocity estimators. It is shown that, when the signal and the noise are assumed to be Poisson processes, both the location and the velocity bounds are inversely proportional to quadratic functions of SNR.

Contents

List of Figures

1 INTRODUCTION

We consider the problem of estimating the location vector $\underline{x}$ and velocity vector $\underline{v}$ of a remote target, as viewed through an optical system. The focal plane consists of a large array of CCD photo-detectors. The amount of charge stored in a CCD cell, after an appropriate exposure time, is the sum of two independent Poisson random variables: one due to the target signal, the other due to noise. Therefore both the signal and the noise are "random" quantities.

Many applications require knowledge of the inherent maximum estimation accuracy. The classical Cramér-Rao lower bound [1,2] has been widely used for this purpose. Using Poisson statistics, Winick in a recent paper [3] has derived the Cramér-Rao location bounds for a stationary target on a two-dimensional CCD focal plane.[1] In this report we investigate the bounds when the target is nonstationary during the time of exposure. As a result of the target motion, the image observed on the focal plane is elongated along the velocity vector.

In this section we discuss a Gaussian-shaped signal model, and in the next section we will derive the Cramér-Rao location and velocity bounds based on this model. We use a two-dimensional Dirac delta function $\delta(\underline{x} - \underline{v}t)$ to represent a rectilinearly moving point source, with $\underline{x}$ and $\underline{v}$ denoting the position and the velocity of the target and t denoting the time. The image of the target is projected upon a CCD focal plane through an ordinary telescope. Let $s_{mn}(\underline{x}, \underline{v})$ be the m-n*th* sample of the optical image, then the relationship between $\delta(\underline{x}, \underline{v}t)$ and $s_{mn}(\underline{x}, \underline{v})$ can be described by linear system as shown in Fig. 1.

Several functions are involved in this system. They are the point-spread function $p(\underline{x})$,

[1] A brief survey of previously published work can be found in Winick's paper [3].

the dimension function of the CCD cell $q_{mn}(\underline{x})$, and the frame integration function $g(t)$.

For the point-spread function we use a Gaussian approximation [4]

$$p(\underline{x}) = \frac{1}{\sqrt{2\pi}\sigma_p} \exp\left[-\frac{\underline{x}'\underline{x}}{2\sigma_p^2}\right] . \tag{1}$$

where σ_p is the standard deviation of the Gaussian function and the prime denotes the transposition operation that converts the column vector into a row vector.

The CCD cells and the temporal integration usually have well defined boundaries. Therefore they should be modeled by a rectangular function. Unfortunately bounds derived from such functions contain integrals which do not have closed form representations. Since a major goal of this work is to derive analytic Cramér-Rao bounds for a special case that is not overly restrictive, so that we can infer some useful properties of the bounds, we will approximate both $q_{mn}(\underline{x})$ and $g(t)$ by Gaussian functions. They are given by

$$q_{mn}(\underline{x}) = \frac{1}{\sqrt{2\pi}\sigma_c} \exp\left[-\frac{(\underline{x} - \underline{x}_{mn})'(\underline{x} - \underline{x}_{mn})}{2\sigma_c^2}\right] \tag{2}$$

and

$$g(t) = \frac{1}{\sqrt{2\pi}\sigma_t} \exp\left[-\frac{t^2}{2\sigma_t^2}\right] . \tag{3}$$

In (2) and (3), σ_c is the radius of a circular area used to approximate the square CCD cell area, and σ_t is a time parameter used to approximate half the frame integration time.

The signal function $s_{mn}(\underline{x}, \underline{y})$, seen by the m-n*th* CCD cell may be obtained by multiplying the Fourier transforms of the four functions and then taking the inverse Fourier transform. The result is

$$s_{mn}(\underline{x}, \underline{y}) = A \exp\left[-\frac{(\underline{x} - \underline{x}_{mn})'(\underline{x} - \underline{x}_{mn})}{2\sigma_s^2}\right] \exp\left[\frac{1}{2}\frac{(\underline{x} - \underline{x}_{mn})'\underline{y}\underline{y}'(\underline{x} - \underline{x}_{mn})}{\sigma_s^2 + \underline{y}'\underline{y}\sigma_t^2}\left(\frac{\sigma_t^2}{\sigma_s^2}\right)\right] , \tag{4}$$

with $\sigma_s^2 = \sigma_c^2 + \sigma_p^2$. In (4) we have used a scaling factor A. If we require that $\sum_{mn} s_{mn}(\underline{x}, \underline{v}) = 1$ then A is given by

$$A = \frac{1}{2\pi\sqrt{\sigma_s^2[\sigma_s^2 + \underline{v}'\underline{v}\sigma_t^2]}} \,. \tag{5}$$

A typical signal image is shown in Fig. 2. Note that the signal has wide spread in the direction of the velocity vector and relatively narrow spread in the perpendicular direction.

Generally Eq. (4) is not a separable function except when the target moves parallel to one of the coordinate axes. Because this simplification allows us to gain some insight into the Cramér-Rao bounds we will formulate the signal for this special case. Let $\underline{x} = [x_1, x_2]$, $\underline{x}_{mn} = [x_{1m}, x_{2n}]$, $\underline{v} = [v_1, v_2]$. Letting $v_2 = 0$ Eq. (4) reduces to a separable function

$$s_{mn}(x_1, x_2, v_1) = P_1(x_1 - x_{1m}, v_1)\, P_2(x_2 - x_{2n}) \tag{6}$$

with P_1 and P_2 given by

$$P_1(x_1 - x_{1m}, v_1) = \frac{1}{\sqrt{2\pi(\sigma_s^2 + v_1^2\sigma_t^2)}} \exp\left[-\frac{(x_1 - x_{1m})^2}{2(\sigma_s^2 + v_1^2\sigma_t^2)}\right] \tag{7}$$

and

$$P_2(x_2 - x_{2n}) = \frac{1}{\sqrt{2\pi\sigma_s^2}} \exp\left[-\frac{(x_2 - x_{2n})^2}{2\sigma_s^2}\right] \,. \tag{8}$$

Eq. (6) will be used in the next section for the derivation of the analytical forms of the Cramér-Rao bounds for the special case of $v_2 = 0$.

2 THE CRAMÉR-RAO BOUNDS

In this section the Cramér-Rao bounds for the estimation of location and velocity are derived. We model the electronic signal (the electron count) $r_{mn}(\underline{x}, \underline{v})$ to be the sum of three independent Poisson processes — the photoelectrons produced by the target, the

photoelectrons produced because of the sky background noise, and the electrons produced by CCD dark-current during frame integration time.[2] The $r_{mn}(\underline{x}, \underline{v})$ itself is therefore a Poisson process[3] with the average number of electrons given by $\lambda_s s_{mn}(\underline{x}, \underline{v}) + \lambda_N$ where λ_s is the average number of photoelectrons produced by a target of unit intensity, and λ_N is the average number of photoelectrons produced by the sum of the two noise processes. The noise is assumed to be spatially and temporally independent and stationary.

If r_{mn} is the observed number of electrons, the likelihood ratio Λ can be written as

$$\Lambda = \Pi_{m,n} \frac{(\lambda_s s_{mn} + \lambda_N)^{r_{mn}} \exp[-(\lambda_s s_{mn} + \lambda_N)]}{\lambda_N^{r_{mn}} \exp[-\lambda_N]} = \Pi_{m,n} \left(1 + \frac{\lambda_s s_{mn}}{\lambda_N}\right)^{r_{mn}} e^{-\lambda_s s_{mn}} . \quad (9)$$

Taking logarithm of both sides, we get the log likelihood ratio

$$\ln \Lambda = \sum_{mn} r_{mn} \ln \left(1 + \frac{\lambda_s s_{mn}}{\lambda_N}\right) - \sum_{mn} \lambda_s s_{mn} . \quad (10)$$

If we assume the stressing case where the target intensity is much less than the noise, that is, $\lambda_s s_{mn} \ll \lambda_N$, [4] then

$$\ln \left(1 + \frac{\lambda_s s_{mn}}{\lambda_N}\right) \approx \frac{\lambda_s s_{mn}}{\lambda_N} . \quad (11)$$

Substituting (11) into (10) yields

$$\ln \Lambda \approx \frac{\lambda_s}{\lambda_N} \sum_{mn} (r_{mn} - \lambda_N) s_{mn} . \quad (12)$$

Eq. (12) provides us with a formula for the matched filter detection of the target streak.

---

[2]The readout circuitry noise is assumed to be small, and not the limiting factor of performance.

[3]Due to the reproductive property of the Poisson distribution.

[4]The bounds derived under this assumption will likely to be too pessimistic when the signal intensity is high.

The Cramér-Rao bounds are the diagonal elements of the inverse of the Fisher information matrix

$$\mathcal{F} = [f_{ij}] \tag{13}$$

where f_{ij}, the i-jth element of $\mathcal{F}$ is defined as

$$f_{ij} = E\left[\frac{\partial \ln \Lambda}{\partial \theta_i}\frac{\partial \ln \Lambda}{\partial \theta_j}\right] . \tag{14}$$

The θ's are defined as $\theta_1 = x_1$, $\theta_2 = x_2$, $\theta_3 = v_1$, and $\theta_4 = v_2$. Therefore, for example, the variance of the x_1 estimate, denoted by $\sigma_{x_1}^2$, satisfies the relationship $\sigma_{x_1}^2 \geq 1/f_{11}$.

Taking the derivative of (12) we obtain

$$\frac{\partial \ln \Lambda}{\partial \theta_i} = \frac{\lambda_s}{\lambda_N}\sum_{mn}(r_{mn} - \lambda_N)\frac{\partial s_{mn}}{\partial \theta_i} . \tag{15}$$

The f_{ij} are then rewritten as

$$\begin{aligned} f_{ij} &= \frac{\lambda_s^2}{\lambda_N^2}E\left[\sum_{mn}(r_{mn} - \lambda_N)\frac{\partial s_{mn}}{\partial \theta_i}\sum_{pq}(r_{pq} - \lambda_N)\frac{\partial s_{pq}}{\partial \theta_j}\right] \\ &= \frac{\lambda_s^2}{\lambda_N^2}\sum_{mn}\sum_{pq}\frac{\partial s_{mn}}{\partial \theta_i}\frac{\partial s_{pq}}{\partial \theta_j}E[(r_{mn} - \lambda_N)(r_{pq} - \lambda_N)] . \end{aligned} \tag{16}$$

Letting $r_{mn} = S_{mn} + N_{mn}$, where S_{mn} and N_{mn} are independent signal and noise processes, then the correlation $E[(r_{mn} - \lambda_N)(r_{pq} - \lambda_N)]$ can be evaluated as

$$\begin{aligned} E[(r_{mn} - \lambda_N)(r_{pq} - \lambda_N)] &= E[(S_{mn} + N_{mn} - \lambda_N)(S_{pq} + N_{pq} - \lambda_N)] \\ &= E[S_{mn}S_{pq}] + E[S_{mn}N_{pq}] - \lambda_N E[S_{mn}] + E[S_{pq}N_{mn}] \\ &\quad + E[N_{mn}N_{pq}] - \lambda_N E[N_{mn}] - \lambda_N E[S_{pq}] - \lambda_N E[N_{pq}] + \lambda_N^2 \\ &= \lambda_s^2 s_{mn}s_{pq} + (\lambda_s s_{mn} + \lambda_N)\delta(m-p, n-q) . \end{aligned} \tag{17}$$

Substituting (17) into (16) yields

$$f_{ij} = \frac{\lambda_s^4}{\lambda_N^2}\sum_{mn}\left(\frac{\partial s_{mn}}{\partial\theta_i}s_{mn}\right)\sum_{pq}\left(\frac{\partial s_{pq}}{\partial\theta_j}s_{pq}\right) + \frac{\lambda_s^3}{\lambda_N^2}\sum_{mn}\left(\frac{\partial s_{mn}}{\partial\theta_i}\frac{\partial s_{mn}}{\partial\theta_j}s_{mn}\right) + \frac{\lambda_s^2}{\lambda_N}\sum_{mn}\left(\frac{\partial s_{mn}}{\partial\theta_i}\frac{\partial s_{mn}}{\partial\theta_j}\right) . \tag{18}$$

The Fisher information matrix, whose elements are given by (18), usually requires numerical computation. However, considerable simplification is possible when the signal is treated as a continuous signal (not sampled) and when its velocity is aligned with one of the axes, owing to the fact that the signal becomes separable. For this special case the Cramér-Rao bounds are found to be[5]

$$\sigma_{x_1}^2 \geq (\sigma_s^2 + v_1^2\sigma_t^2)\Big/\left[\frac{4\mathrm{SNR}^2}{9\lambda_s} + \frac{\mathrm{SNR}}{2}\right] , \tag{19}$$

$$\sigma_{x_2}^2 \geq \sigma_s^2\Big/\left[\frac{4\mathrm{SNR}^2}{9\lambda_s} + \frac{\mathrm{SNR}}{2}\right] , \tag{20}$$

$$\sigma_{v_1}^2 \geq \left(\frac{\sigma_s^2 + v_1^2\sigma_t^2}{v_1\sigma_t^2}\right)^2\Big/\left[\left(\frac{1}{4} + \frac{8}{9\lambda_s}\right)\mathrm{SNR}^2 + \frac{3\mathrm{SNR}}{4}\right] . \tag{21}$$

The SNR is the signal-to-noise ratio defined as the ratio of the signal energy and the noise variance. For the separable signal in (6) we have

$$\mathrm{SNR} = \frac{\lambda_s^2}{4\pi\sigma_s\sqrt{\sigma_s^2 + v_1^2\sigma_t^2}\lambda_N} . \tag{22}$$

After appropriate normalizations to render the bounds dimensionless we obtain

$$\left(\frac{\sigma_{x_1}}{\sigma_s}\right)^2 \geq \left[1 + v_1^2\left(\frac{\sigma_t}{\sigma_s}\right)^2\right]\Big/\left[\frac{4\mathrm{SNR}^2}{9\lambda_s} + \frac{\mathrm{SNR}}{2}\right] , \tag{23}$$

$$\left(\frac{\sigma_{x_2}}{\sigma_s}\right)^2 \geq 1\Big/\left[\frac{4\mathrm{SNR}^2}{9\lambda_s} + \frac{\mathrm{SNR}}{2}\right] , \tag{24}$$

$$\left(\frac{\sigma_{v_1}}{\sigma_s/\sigma_t}\right)^2 \geq \frac{1}{v_1^2}\left(\frac{\sigma_s}{\sigma_t}\right)^2\left[1 + v_1^2\left(\frac{\sigma_t}{\sigma_s}\right)^2\right]^2\Big/\left[\left(\frac{1}{4} + \frac{8}{9\lambda_s}\right)\mathrm{SNR}^2 + \frac{3\mathrm{SNR}}{4}\right] . \tag{25}$$

[5]Derivation of the bounds is given in Appendix A.

Letting $\sigma_p = 1$ and $\sigma_c = \frac{1}{2}$ (thus $\sigma_s^2 = 1.25$), and $\sigma_t = \frac{1}{2}$, and $\lambda_s = 1$ we plot the bounds of σ_{x_1} and σ_{v_1} for different velocities and signal-to-noise ratios in Fig. 3. In Fig. 4 we plot the bounds for different λ_s, setting SNR = 10 dB.

We observe that

1. The bounds are functions of SNR as well as λ_s (or equivalently, λ_N).

2. The bounds (of the variances) are inversely proportional to quadratic functions of SNR.

3. For fixed SNR the bounds increase monotonically as λ_s increases. This property can be explained by observing that if λ_s increases linearly λ_N must increase quadratically to keep SNR constant.

4. All bounds are independent of the target location.

In Fig. 5 we have plotted a few typical location and velocity bounds to illustrate the relationship between the bounds and the target velocity. It can be verified that the location bound increases monotonically between $v_1 = 0$ and $v_1 = \infty$ and that the velocity bound has a minimum somewhere in the interval $[0.707\sigma_s/\sigma_t, 0.816\sigma_s/\sigma_t]$. Thus, as a design criterion, σ_s/σ_t should be chosen in the vicinity of expected target velocity – the classic dwell-in-cell criterion.

In appendix B we have included formulas for the numerical computation of the Cramér-Rao bounds. The computed Cramér-Rao bounds have similar behaviors as those discovered for the special case of $v_2 = 0$ discovered in the section.

3 SUMMARY AND DISCUSSION

For a moving point target we have derived the Cramér-Rao bounds for the variance of the location and velocity estimators. The major difference between our result and previously published works is that during the CCD exposure time, the target streaks and the velocity parameter must be estimated from the streak.

To compare our results with [3] let us set $v_1 = 0$ in (A8). The location bound can be rewritten as

$$\frac{\sigma_x^2 \lambda_s}{\sigma_p^2} \geq \frac{72\pi^2 \left(\sigma_p^2 + \sigma_c^2\right)^3}{(\lambda_s/\lambda_N)^2[2 + 9\pi(\sigma_p^2 + \sigma_c^2)\lambda_N/\lambda_s]\sigma_p^2} . \tag{26}$$

If we fix σ_c, the size of the CCD cells, and vary σ_p, the size of the point-spread function, it can be shown that (26) approaches infinity when σ_p approaches either zero or infinity, and that (26) has a minimum when σ_c/σ_p is in the vicinity of 1. Some typical curves of (26) are plotted on the left hand side of Fig. 6. This is essentially what is shown in Fig. 2 of [3]. However, we notice that as σ_p approaches zero both sides of of (26) approach infinity regardless of the value of σ_x^2. That is, the normalization by σ_p^2 masks the true behavior of the bound when the point-spread function becomes infinitesimal. A more interesting asymptotic behavior, however, is obtained when we normalize (A8) differently, namely

$$\frac{\sigma_x^2 \lambda_s}{\sigma_p^2 + \sigma_c^2} \geq \frac{72\pi^2 \left(\sigma_p^2 + \sigma_c^2\right)^2}{(\lambda_s/\lambda_N)^2[2 + 9\pi(\sigma_p^2 + \sigma_c^2)\lambda_N/\lambda_s]} . \tag{27}$$

The right hand side of (27) approaches infinity as σ_p approaches infinity, but it approaches a finite value when σ_p approaches zero. Some typical curves of (27) are plotted on the right hand side of Fig. 6. Intuitively, if the point-spread function is much wider than the CCD cell size system performance suffers because we must look at many noisy pixels in order to collect most of the signal energy in the spot. On the other hand, if the point-spread

function is much smaller than the cell size, we lose subpixel resolution, and therefore the bound asymptotically approaches a finite value.

ACKNOWLEDGEMENT

The author would like to thank Dr. A. E. Filip and Dr. K. P. Dunn of MIT Lincoln Laboratory for their many useful discussions.

APPENDICES

A THE FISHER INFORMATION MATRIX – $v_2 = 0$

To evaluate the Fisher information matrix we must find the derivatives of the signal function. In the special case that $v_2 = 0$ the signal is given by

$$s_{mn}(x_1, x_2, v_1) = P_1(x_1 - x_{1m}, v_1)\, P_2(x_2 - x_{2n}) \,, \tag{A1}$$

where

$$P_1(x_1 - x_{1m}, v_1) = \frac{1}{\sqrt{2\pi(\sigma_s^2 + v_1^2\sigma_t^2)}} \exp\left[-\frac{(x_1 - x_{1m})^2}{2(\sigma_s^2 + v_1^2\sigma_t^2)}\right] \tag{A2}$$

and

$$P_2(x_2 - x_{2n}) = \frac{1}{\sqrt{2\pi\sigma_s^2}} \exp\left[-\frac{(x_2 - x_{2n})^2}{2\sigma_s^2}\right] \,. \tag{A3}$$

The derivatives of Eq. (A1) are

$$\frac{\partial s_{mn}}{\partial x_1} = -\frac{x_1 - x_{1m}}{\sigma_s^2 + v_1^2\sigma_t^2} P_1(x_1 - x_{1m}, v_1) P_2(x_2 - x_{2n}) \,, \tag{A4}$$

$$\frac{\partial s_{mn}}{\partial x_2} = -\frac{x_2 - x_{2n}}{\sigma_s^2} P_1(x_1 - x_{1m}, v_1) P_2(x_2 - x_{2n}) \,, \text{ and} \tag{A5}$$

$$\frac{\partial s_{mn}}{\partial v_1} = \frac{v_1\sigma_t^2}{\sigma_s^2 + v_1^2\sigma_t^2}\left[\frac{(x_1 - x_{1m})^2}{\sigma_s^2 + v_1^2\sigma_t^2} - 1\right] P_1(x_1 - x_{1m}, v_1) P_2(x_2 - x_{2n}) \,. \tag{A6}$$

In the following we assume that all summations can be replaced by corresponding integrals, this corresponds to the limiting case of small detector cells and large focal plane. Some useful summations are

$$\sum P^2 = \frac{1}{2\sqrt{\pi}\sigma} \,, \quad \sum x^2 P^2 = \frac{\sigma}{4\sqrt{\pi}} \,, \quad \sum x^4 P^2 = \frac{3\sigma^3}{8\sqrt{\pi}} \,,$$

$$\sum P^3 = \frac{1}{2\sqrt{3\pi}\sigma^2} \,, \quad \sum x^2 P^3 = \frac{1}{6\sqrt{3\pi}} \,, \quad \sum x^4 P^3 = \frac{\sigma^2}{6\sqrt{3\pi}} \,,$$

where P, x, and σ^2 are either $P_1(x_1 - x_{1m}, v_1)$, $x_1 - x_{1m}$, and $\sigma_s^2 + v_1^2\sigma_t^2$ or $P_2(x_2 - x_{2n})$, $x_2 - x_{2n}$, and σ_s^2.

The energy of the electronic signal is given by

$$\begin{aligned} E &= \lambda_s^2 \sum_{mn} P_1^2(x_1 - x_{1m}, v_1) P_2^2(x_2 - x_{2n}) \\ &= \frac{\lambda_s^2}{4\pi\sigma_s\sqrt{\sigma_s^2 + v_1^2\sigma_t^2}} . \end{aligned} \tag{A7}$$

The SNR is defined to be the ratio of signal energy and noise variance, namely, E/λ_N. A justification of using this definition, based on hypothesis testing theory, is given in Appendix C.

We now derive the elements of the Fisher information matrix. Because s_{mn} and $\partial s_{mn}/\partial v_1$ are even functions in m and n and $\partial s_{mn}/\partial x_1$ and $\partial s_{mn}/\partial x_2$ are odd functions and all four functions are separable, the first term in Eq. (18) is equal to zero except when $\theta_i = \theta_j = v_1$, the second and the third terms also are equal to zero except when $\theta_i = \theta_j = x_1$ or when $\theta_i = \theta_j = x_2$ or when $\theta_i = \theta_j = v_1$. Therefore all of the off diagonal terms of the Fisher information matrix are equal to zero and the diagonal terms are given by, after some algebraic manipulation,

$$\begin{aligned} f_{11} &= \frac{\lambda_s^3}{\lambda_N^2} \sum_{mn} \left(\frac{\partial s_{mn}}{\partial x_1}\right)^2 s_{mn} + \frac{\lambda_s^2}{\lambda_N} \sum_{mn} \left(\frac{\partial s_{mn}}{\partial x_1}\right)^2 \\ &= \frac{\lambda_s^2}{\lambda_N^2} \left[\frac{\lambda_s}{36\pi^2\sigma_s^2(\sigma_s^2 + v_1^2\sigma_t^2)^2} + \frac{\lambda_N}{8\pi\sigma_s(\sigma_s^2 + v_1^2\sigma_t^2)^{3/2}} \right] , \end{aligned} \tag{A8}$$

$$\begin{aligned} f_{22} &= \frac{\lambda_s^3}{\lambda_N^2} \sum_{mn} \left(\frac{\partial s_{mn}}{\partial x_2}\right)^2 s_{mn} + \frac{\lambda_s^2}{\lambda_N} \sum_{mn} \left(\frac{\partial s_{mn}}{\partial x_2}\right)^2 \\ &= \frac{\lambda_s^2}{\lambda_N^2} \left[\frac{\lambda_s}{36\pi^2\sigma_s^4(\sigma_s^2 + v_1^2\sigma_t^2)} + \frac{\lambda_N}{8\pi\sigma_s^3\sqrt{\sigma_s^2 + v_1^2\sigma_t^2}} \right] , \end{aligned} \tag{A9}$$

$$f_{33} = \frac{\lambda_s^4}{\lambda_N^2} \left(\sum_{mn} \frac{\partial s_{mn}}{\partial v_1} s_{mn} \right)^2 + \frac{\lambda_s^3}{\lambda_N^2} \sum_{mn} \left(\frac{\partial s_{mn}}{\partial v_1}\right)^2 s_{mn} + \frac{\lambda_s^2}{\lambda_N} \sum_{mn} \left(\frac{\partial s_{mn}}{\partial v_1}\right)^2$$

$$= \frac{\lambda_s^2}{\lambda_N^2}\left[\frac{\lambda_s^2}{4}+\frac{8\lambda_s}{9}+3\lambda_N\pi\sqrt{\sigma_s^2+v_1^2\sigma_t^2}\sigma_s\right]\frac{(v_1\sigma_t^2)^2}{16\pi^2(\sigma_s^2+v_1^2\sigma_t^2)^3\sigma_s^2}\,. \qquad \text{(A10)}$$

After rewriting f_{11}, f_{22}, and f_{33} in terms of SNR we conclude that the Fisher information matrix for the special case that $v_2 = 0$ is

$$\mathcal{F} = \begin{bmatrix} \left(\frac{4\mathrm{SNR}^2}{9\lambda_s}+\frac{\mathrm{SNR}}{2}\right)\frac{1}{\sigma_s^2+v_1^2\sigma_t^2} & 0 & 0 \\ 0 & \left(\frac{4\mathrm{SNR}^2}{9\lambda_s}+\frac{\mathrm{SNR}}{2}\right)\frac{1}{\sigma_s^2} & 0 \\ 0 & 0 & \left[\left(\frac{1}{4}+\frac{8}{9\lambda_s}\right)\mathrm{SNR}^2+\frac{3}{4}\mathrm{SNR}\right]\left(\frac{v_1\sigma_t^2}{\sigma_s^2+v_1^2\sigma_t^2}\right)^2 \end{bmatrix} \qquad \text{(A11)}$$

B FORMULAS FOR THE COMPUTATION OF C-R BOUNDS

To compute the Cramér-Rao bounds numerically the following derivatives of (4) are needed:

$$\frac{\partial s_{mn}}{\partial x_1} = -\left\{\frac{x_1-x_{1m}}{\sigma_s^2}-\frac{[v_1(x_1-x_{1m})+v_2(x_2-x_{2n})]\,v_1}{\sigma_s^2+(v_1^2+v_2^2)\sigma_t^2}\frac{\sigma_t^2}{\sigma_s^2}\right\}s_{mn}\,, \qquad \text{(B1)}$$

$$\frac{\partial s_{mn}}{\partial x_2} = -\left\{\frac{x_2-x_{2n}}{\sigma_s^2}-\frac{[v_1(x_1-x_{1m})+v_2(x_2-x_{2n})]\,v_2}{\sigma_s^2+(v_1^2+v_2^2)\sigma_t^2}\frac{\sigma_t^2}{\sigma_s^2}\right\}s_{mn}\,, \qquad \text{(B2)}$$

$$\frac{\partial s_{mn}}{\partial v_1} = -\left\{\frac{v_1\sigma_t^2}{\sigma_s^2+(v_1^2+v_2^2)\sigma_t^2}-\frac{[v_1(x_1-x_{1m})+v_2(x_2-x_{2n})](x_1-x_{1m})}{\sigma_s^2+(v_1^2+v_2^2)\sigma_t^2}\frac{\sigma_t^2}{\sigma_s^2}\right.$$
$$\left.+\frac{[v_1(x_1-x_{1m})+v_2(x_2-x_{2n})]^2\,v_1}{[\sigma_s^2+(v_1^2+v_2^2)\sigma_t^2]^2}\frac{\sigma_t^4}{\sigma_s^2}\right\}s_{mn}\,, \qquad \text{(B3)}$$

$$\frac{\partial s_{mn}}{\partial v_2} = -\left\{\frac{v_2\sigma_t^2}{\sigma_s^2+(v_1^2+v_2^2)\sigma_t^2}-\frac{[v_1(x_1-x_{1m})+v_2(x_2-x_{2n})](x_2-x_{2n})}{\sigma_s^2+(v_1^2+v_2^2)\sigma_t^2}\frac{\sigma_t^2}{\sigma_s^2}\right.$$
$$\left.+\frac{[v_1(x_1-x_{1m})+v_2(x_2-x_{2n})]^2\,v_2}{[\sigma_s^2+(v_1^2+v_2^2)\sigma_t^2]^2}\frac{\sigma_t^4}{\sigma_s^2}\right\}s_{mn}\,. \qquad \text{(B4)}$$

We can rewrite (18) as an explicit function of SNR

$$f_{ij} = \mathrm{SNR}^2\left(\sum_{mn}\frac{\partial s_{mn}}{\partial\theta_i}s_{mn}\sum_{pq}\frac{\partial s_{pq}}{\partial\theta_j}s_{pq}+\frac{1}{\lambda_s}\sum_{mn}\frac{\partial s_{mn}}{\partial\theta_i}\frac{\partial s_{mn}}{\partial\theta_j}s_{mn}\right)\Big/\left(\sum_{mn}s_{mn}^2\right)^2$$
$$+\mathrm{SNR}\left(\sum_{mn}\frac{\partial s_{mn}}{\partial\theta_i}\frac{\partial s_{mn}}{\partial\theta_j}\right)\Big/\left(\sum_{mn}s_{mn}^2\right)\,. \qquad \text{(B5)}$$

where $\theta_1 = x_1$, $\theta_2 = x_2$, $\theta_3 = v_1$, and $\theta_4 = v_2$.

C THE SNR AS A PERFORMANCE PARAMETER

In this appendix we relate our choice of SNR to a hypothesis testing performance parameter. Using (9), and denoting the hypothesis of no signal present by H_0, it can be shown that

$$E[\Lambda|H_0] = 1 , \tag{C1}$$

$$\begin{aligned} E[\Lambda^2|H_0] &= \prod_{mn} E\left[\left(1+\frac{\lambda_s s_{mn}}{\lambda_N}\right)^{2r_{mn}}\right] \exp\left(-2\lambda_s s_{mn}\right) \\ &= \prod_{mn} \exp\left(2\lambda_s s_{mn} + \frac{\lambda_s^2 s_{mn}^2}{\lambda_N}\right) \exp\left(-2\lambda_s s_{mn}\right) \\ &= \prod_{mn} \exp\left[\frac{\lambda_s^2 s_{mn}^2}{\lambda_N}\right] . \end{aligned} \tag{C2}$$

We denote the distance between the means of the conditional densities $p(\Lambda|H_0)$ and $p(\Lambda|H_1)$ by d. The d is commonly used to characterize the test performance and d^2 is given by (p.137, [5],[6])

$$d^2 = \ln\{1 + \mathrm{VAR}(\Lambda|H_0)\} = \ln\{E[\Lambda^2|H_0]\} . \tag{C3}$$

Substituting (C2) into (C3) yields

$$d^2 = \sum_{mn} \frac{\lambda_s^2 s_{mn}^2}{\lambda_N} , \tag{C4}$$

which is identical to our definition of SNR.

References

[1] J. M. Wozencraft and I. M. Jacobs, Principles of Communication Engineering. New York: Wiley, 1965.

[2] H. Cramer, Mathematical Methods of Statistics. Princeton, N.J: Princeton University Press, 1946.

[3] K. A. Winick, "Cramér-Rao lower bounds on the performance of charge-coupled-device optical position estimators," J. Opt. Soc. of Am., vol. 3, pp. 1809-1815; November 1986.

[4] K. Seyrafi, "Electro-optical systems analysis," Electro-Optical Research Company, Los Angeles, 1973.

[5] H. Van Trees, Detection, Estimation and Modulation Theory, Wiley, New York, 1968, Part I.

[6] W. W. Peterson, T. G. Birdsall, and W. C. Fox,"The theory of signal detectability," pp.171-212, PGIT-4, IRE Trans. Information Theory, 1954.

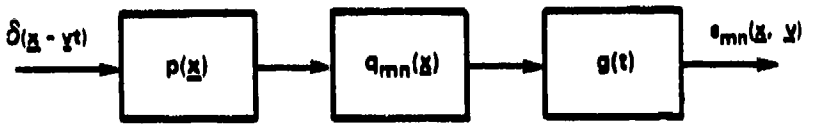

87686-1

Figure 1. The linear system of optical image generation.

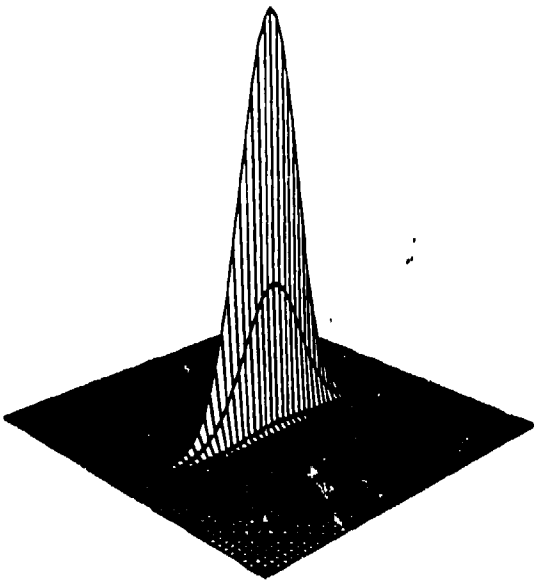

87685-2

Figure 2. A typical signal image.

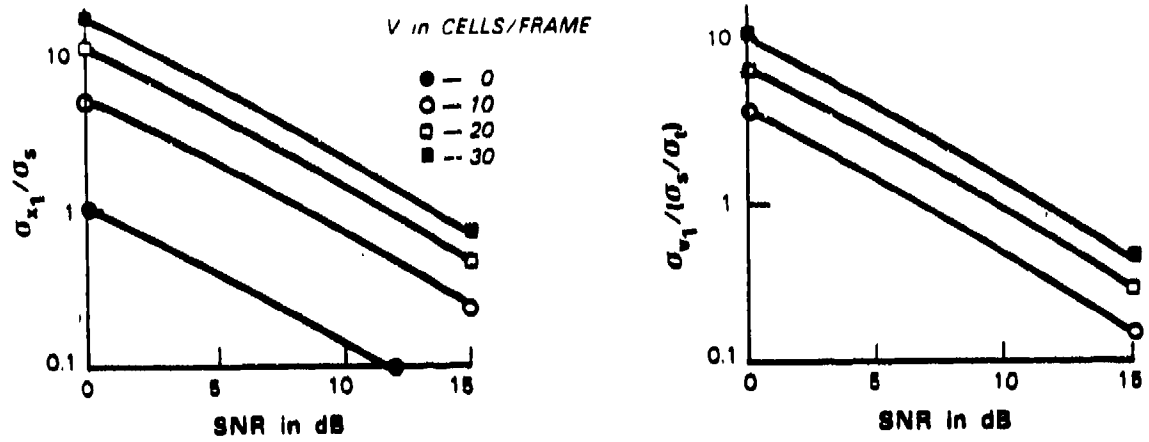

Figure 3. The Cramér-Rao bounds($\lambda_s = 1$).

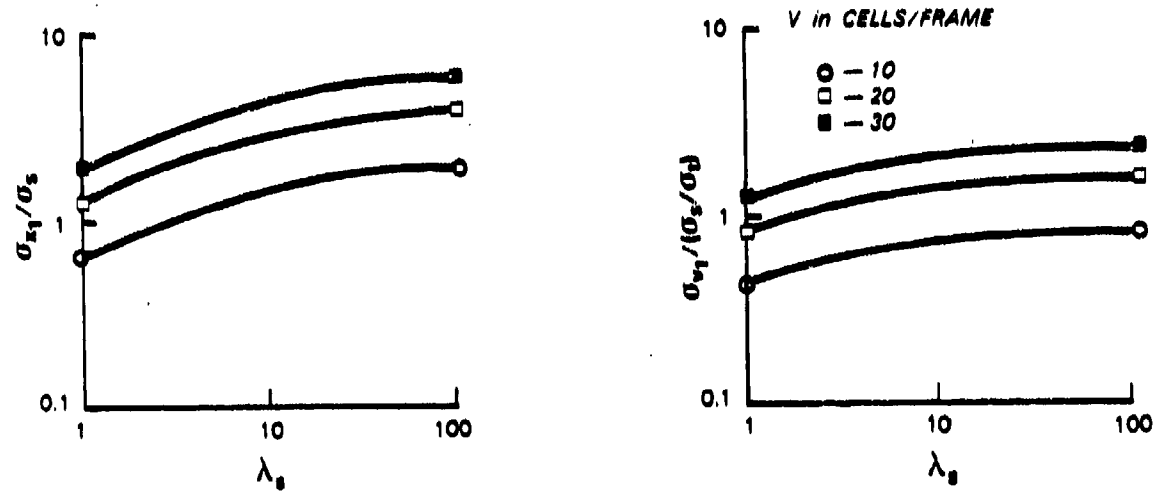

Figure 4. The Cramér-Rao bounds(SNR = 10 dB).

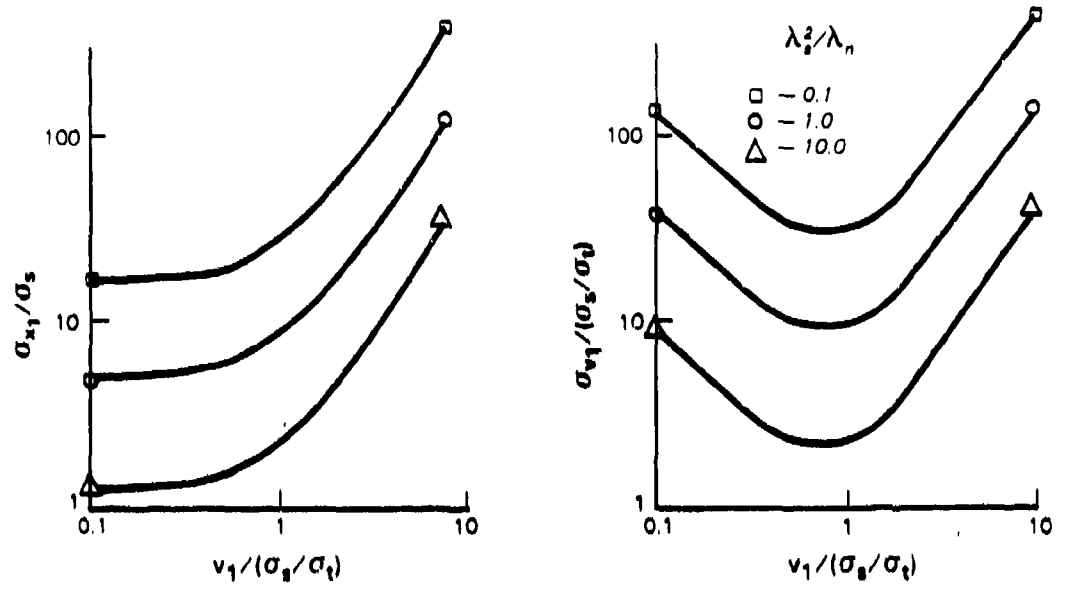

87595-5

Figure 5. Some typical bounds versus target velocity ($\lambda_s = 1$).

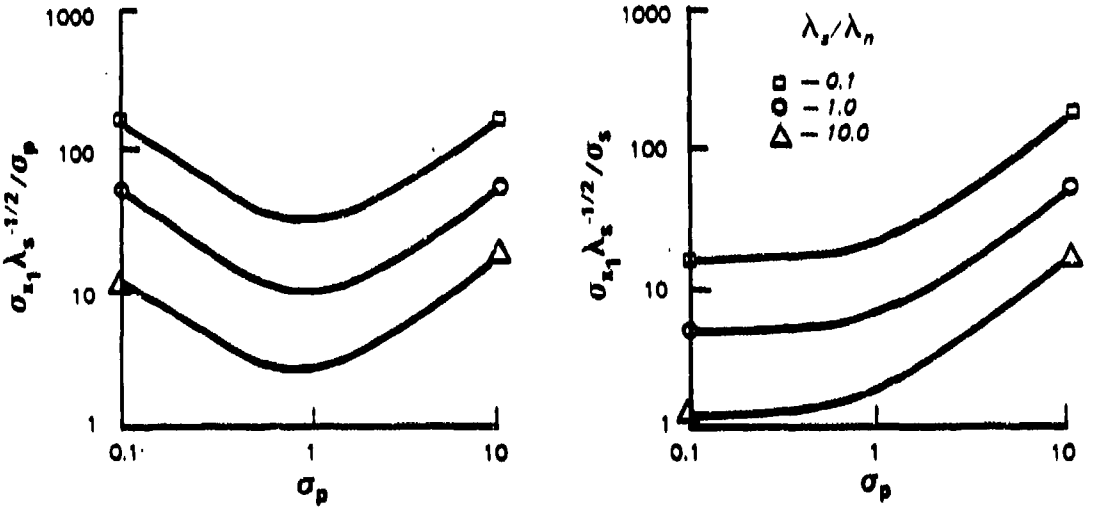

87596-6

Figure 6. The location bounds for stationary targets ($\lambda_s = 1$).

UNCLASSIFIED

SECURITY CLASSIFICATION OF THIS PAGE

REPORT DOCUMENTATION PAGE

1a. REPORT SECURITY CLASSIFICATION Unclassified	1b. RESTRICTIVE MARKINGS
2a. SECURITY CLASSIFICATION AUTHORITY	3. DISTRIBUTION/AVAILABILITY OF REPORT Approved for public release; distribution unlimited.
2b. DECLASSIFICATION/DOWNGRADING SCHEDULE	
4. PERFORMING ORGANIZATION REPORT NUMBER(S) Technical Report 777	5. MONITORING ORGANIZATION REPORT NUMBER(S) ESD-TR-87-082
6a. NAME OF PERFORMING ORGANIZATION Lincoln Laboratory, MIT 6b. OFFICE SYMBOL *(If applicable)*	7a. NAME OF MONITORING ORGANIZATION Electronic Systems Division
6c. ADDRESS *(City, State, and Zip Code)* P.O. Box 73 Lexington, MA 02173-0073	7b. ADDRESS *(City, State, and Zip Code)* Hanscom AFB, MA 01731
8a. NAME OF FUNDING/SPONSORING ORGANIZATION Air Force 8b. OFFICE SYMBOL *(If applicable)* AFSTL	9. PROCUREMENT INSTRUMENT IDENTIFICATION NUMBER F19628-85-C-0002
8c. ADDRESS *(City, State, and Zip Code)* Air Force Systems Command, USAF Andrews Air Force Base Washington, DC 20334	10. SOURCE OF FUNDING NUMBERS PROGRAM ELEMENT NO.: 63220C PROJECT NO.: TASK NO.: WORK UNIT ACCESSION NO.:

11. TITLE *(Include Security Classification)*

Cramér-Rao Bounds on the Accuracy of Location and Velocity Estimations Using CCD Optical Sensors

12. PERSONAL AUTHOR(S)
Yeunung Chen

13a. TYPE OF REPORT	13b. TIME COVERED	14. DATE OF REPORT *(Year, Month, Day)*	15. PAGE COUNT
Technical Report	FROM _____ TO _____	2 November 1987	28

16. SUPPLEMENTARY NOTATION
None

17. COSATI CODES		
FIELD	GROUP	SUB-GROUP

18. SUBJECT TERMS *(Continue on reverse if necessary and identify by block number)*
CCD Imaging; parameter estimation; Cramér-Rao Bounds; point spread function

19. ABSTRACT *(Continue on reverse if necessary and identify by block number)*

A moving point-target generates a non-circular image on a CCD photo-detector focal plane. Using a two-dimensional Gaussian signal model, we have derived the Cramér-Rao lower bounds for target location and velocity estimators. It is shown that, when the signal and the noise are assumed to be Poisson processes, both the location and the velocity bounds are inversely proportional to quadratic functions of SNR.

20. DISTRIBUTION/AVAILABILITY OF ABSTRACT	21. ABSTRACT SECURITY CLASSIFICATION
☐ UNCLASSIFIED/UNLIMITED ☒ SAME AS RPT. ☐ DTIC USERS	Unclassified

22a. NAME OF RESPONSIBLE INDIVIDUAL	22b. TELEPHONE *(Include Area Code)*	22c. OFFICE SYMBOL
Lt. Col. Hugh L. Southall, USAF	(617) 863-5500, Ext. 2330	ESD/TML

DD FORM 1473, 84 MAR — 83 APR edition may be used until exhausted. All other editions are obsolete.

UNCLASSIFIED

SECURITY CLASSIFICATION OF THIS PAGE